Three-Dimensional Structure of the mesoscale eddies in the Agulhas Current region from hydrological and altimetry data

N. V. Sandalyuk[1] and T. V. Belonenko[1]

In this work by implementing the method of colocalization the altimetry data and temperature and salinity profiles we provide a detailed study of the averaged thermohaline structure of the anticyclonic and cyclonic mesoscale eddies formed in the southern part of the Agulhas Current system. The observed intensification of eddy dissipation processes can be caused by the topographic barriers, such as the Agulhas Plateau or the Agulhas Ridge. In the eddies of both polarities significant temperature anomalies are concentrated within the distance of one radius from the eddy center and to the depth of ~ 1500 m. The obtained averaged estimates of heat and salt transported by the Agulhas Rings is 2.38×10^{20} J and 4.79×10^{12} kg respectively. Westward propagation of the zonal eddy-induced transport for anticyclonic and cyclonic eddies is observed in the Agulhas Retroflection region, Cape Basin and in the central part of the shelf zone with the maximum values of 4 Sv/deg^2 for anticyclonic eddies and 1.77 Sv/deg^2 for cyclonic eddies. *KEYWORDS:* Agulhas Rings; Agulhas Current; mesoscale eddies; altimetry; three-dimensional structure.

Citation: Sandalyuk, N. V. and T. V. Belonenko (2021), Three-Dimensional Structure of the mesoscale eddies in the Agulhas Current region from hydrological and altimetry data, *Russ. J. Earth. Sci., 21*, ES4005, doi:10.2205/2021ES000764.

Introduction

Although mesoscale eddies are ubiquitous in the World Ocean [*Chelton et al.,* 2007, 2011], the areas of highest eddy activity are confined to the regions of large-scale currents due to the baroclinic and barotropic instability, which is one of the main conditions for eddy generation [*Monin and Zhikharev,* 1990]. In the Southern Hemisphere, such currents are the Brazilian, East Australian, Antarctic Circumpolar Current, and the Agulhas Current.

In this work, we provide a detailed study of the general thermohaline structure of the mesoscale eddies formed in the southern part of the Agulhas

Current system. This region is one of the most dynamically complex areas of the World's Oceans. It is characterized by the high variability of thermohaline fields over a wide range of space-time scales [*Lutjeharms,* 2006: *Lutjeharms and Ballegooyen,* 1988].

In the Agulhas Retroflection area, the Agulhas Current turns back on itself and flows eastward forming a loop from which the large anticyclonic rings are detaching (Figure 1). These rings are responsible for the transfer of warmer and saltier Indian Ocean waters to the South Atlantic [*Lutjeharms and Ballegooyen,* 1988; *Lutjeharms and Valentine,* 1988]. The main distinctions of the Agulhas Rings from other eddies are larger spatial scales, longer lifespans, and their predominant northwestern propagation direction [*Boebel et al.,* 2003; *Dencausse et al.,* 2010; *Lutjeharms,* 2007; *Malysheva et al.,* 2018; *Sandalyuk et al.,* 2018; *van Sebille and van Leeuwen,* 2007].

---

[1]Saint Petersburg State University, St. Petersburg, Russia
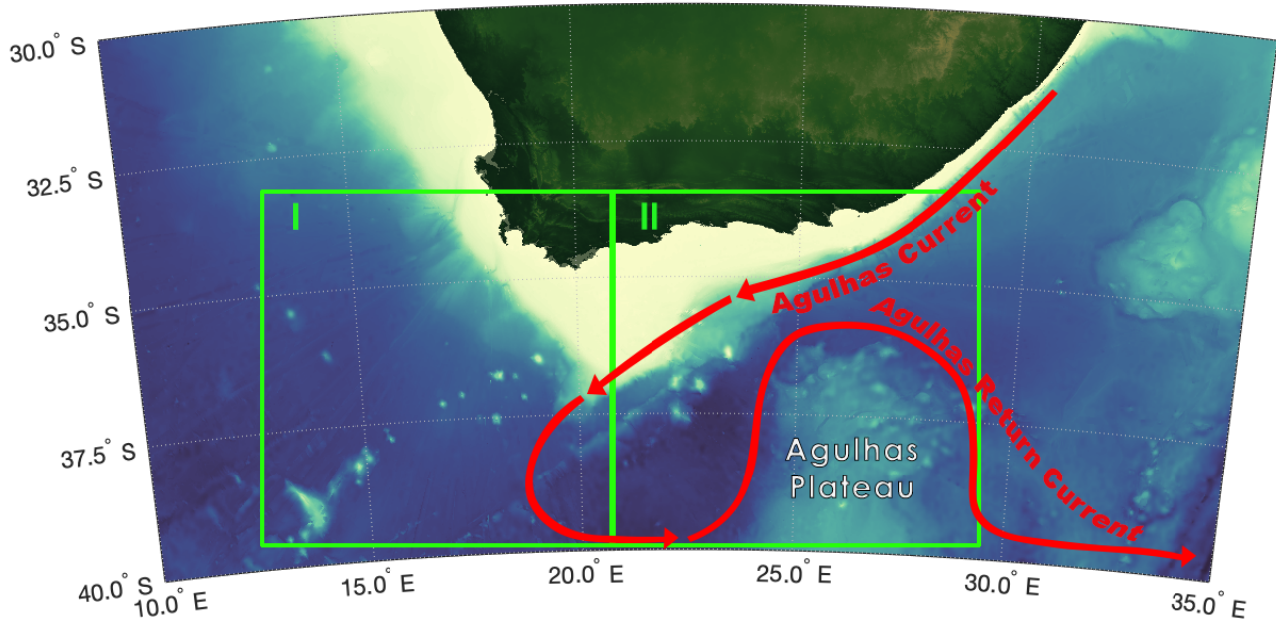
Figure 1. Agulhas Current region with the bathymetry (ETOPO1 1 Arc-Minute Global Relief Model) and schematic path of the Agulhas Current system. I and II – regions selected for the analysis of the composite eddy structure.

The Agulhas Rings have previously been investigated in a number of studies [e.g. *van Ballegooyen et al., 1994*; *Byrne et al., 1995*; *Gordon et al., 1987*; *Laxenaire et al., 2019*; *McCartney and Woodgate-Jones, 1991*; *Schouten et al., 2000*; *Schmid et al., 2003*]. These studies confirm the crucial role of the Agulhas Rings in the Indo-Atlantic interocean exchange of heat and salt.

It should be noted that in previous studies the thermohaline structure of the Agulhas Rings has been analyzed on the example of the individual eddies while in our study we evaluate the eddy structure by obtaining composite anticyclonic eddy, which represents the averaged structure of the Agulhas Rings. A similar technique for studying Agulhas Rings was implemented in the work of *Souza et al.* [2011]. In our research, we use results of the new advanced eddy automatic identification method, which covers a wider time range and significantly larger amount of profiles.

In this paper we focus on the general thermohaline structure of the Agulhas Rings and their contribution to the heat and salt transport in the study region. However, we also asses the three-dimensional structure of the anticyclonic eddies

which form in the Agulhas Current region but not associated with the Agulhas Rings. Moreover, we analyze three-dimensional structure of the cyclonic eddies forming in the study region.

2. Data and Methods

2.1. Mesoscale Eddy Trajectory Atlas Product

To identify the position of mesoscale eddies and track their propagation, the "Mesoscale Eddy Trajectory Atlas Product" data set was used. This data set based on the algorithm developed by *Chelton et al.* [2011] and applied to SLA fields from merged multimission satellite measurements. The algorithm was modified as described in *Schlax and Chelton* [2016] based on the approach described by *Williams et al.* [2011]. The "growing" method of eddy identification defines the anticyclonic eddy interior by finding a local maximum in SLA and all neighboring pixels whose SLA values lie above a sequence of decreasing thresholds. This "growth" of the eddy interior is continued until at least one of the criteria for this coherent structure is violated. Cyclonic eddies are defined in the same way

by finding the local minimum of SSH [*Schlax and Chelton,* 2016]. The dataset is now routinely generated and quality-controlled by the Data Unification and Altimeter Combination System (DUACS) and distributed by AVISO+. The dataset and the documentation with a detailed description of the modified algorithm are available at https://www.aviso.altimetry.fr. The final version of the dataset contains the location of detected eddies on each day for the whole altimetry period (1993–ongoing).

2.2. ARGO Data

To construct three-dimensional composite structure of mesoscale eddies in the Agulhas Current system region, the ARGO temperature and salinity profiles were used. The data is available at the Coriolis Data Center website (http://www.coriolis.eu.org/Observing-the-Ocean/ARGO). Only profiles flagged "ADJUSTED" were used in the research. It is a delayed mode data which means that profiles have been subjected to detailed scrutiny by oceanographic experts and the adjusted salinity has been estimated by comparison with high-quality ship-based CTD data and climatologies. Only profiles with pressure, temperature, and salinity data flagged as good were used in the analysis. In addition, the more rigorous quality control was implemented to exclude "suspicious" profiles. The profiles with the last record shallower than 500 m were eliminated [*Chaigneau et al.,* 2011; *He et al.,* 2018]. After the implementation of all levels of quality control, the 9179 profiles were obtained for the study region for the period of 2000–2018. The retained profiles were linearly interpolated onto 5 m regular grid: from 0 to 1500 m.

## 2.3. Construction of the Composite Three-Dimensional Structures

The method of colocalization the altimetry and *in situ* data was presented in *Willis and Fu* [2008] and *Chaigneau et al.* [2011] and been extensively used in a number of studies covering different regions of the World Ocean [e.g. *Dong et al.,* 2017; *He et al.,* 2018; *Keppler et al.,* 2018; *Kubryakov et al.,* 2018; *Sandalyuk et al.,* 2020; *Yang et al.,* 2013; *Yu et al.,* 2017].

Each selected profile was associated with the nearest eddy if it satisfied the two following conditions: (1) The profile and the eddy have the same observation day; (2) The profile located within a distance less than the eddy radius R derived from the "Mesoscale Eddy Trajectory Atlas Product". The distance between the location of the profile and the eddy center was normalized by the radius R. Normalized distance 0 corresponds to the eddy center while normalized distance 1 corresponds to the eddy maximum velocity average within the contour defining the eddy. This approach is based on the assumption made by *Zhang et al.* [2013] that all eddies, regardless of their amplitude, polarity or scale have the same structure, therefore we can expect that the dependence of the eddy's thermohaline structure on its radius is universal for eddies of different scales. Subsequent works that followed that technique confirmed the feasibility of this approach [e.g. *He et al.,* 2018; *Kubryakov et al.,* 2018; *Keppler et al.,* 2018; *Sandalyuk et al.,* 2020]. However, we increase the size of the composite eddy to $1.5R$ as the presence of eddies also influences its vicinity [*He et al.,* 2018].

Analyzed profiles were classified into two groups depending on the vorticity sign: anticyclonic (AE) and cyclonic (CE). The total number of profiles located within the distance of $1.5R$ from the center for AEs and CEs is 1193 and 1159. Figure 2 displays the distribution of the obtained profiles in the normalized eddy-coordinate system.

In order to better understand the vertical thermohaline structure of the mesoscale eddies and estimate zonal transport induced by CEs and AEs, the temperature (T') and salinity (S') anomalies were calculated by subtracting monthly local mean climatological T/S profiles from T/S profiles associated with the eddies. The mean climatology was computed from the hydrographical data set within $2.5R$ around each eddy observation. To construct three-dimensional composite eddy structure retained T'/S' profiles were finally interpolated onto a regular $0.1 \times 0.1R$ grid at each depth level (5 m) using Barnes objective analysis with the smoothing length scale of 0.5 for both radial and vertical axis [*Barnes,* 1973; *Keppler et al.,* 2018].

To achieve an estimation on spatial distribution of the zonal and meridional eddy induced volume transport we follow the approach of *Dong et al.* [2017], who proposed a new method for eddy heat and salt transport evaluation using eddy
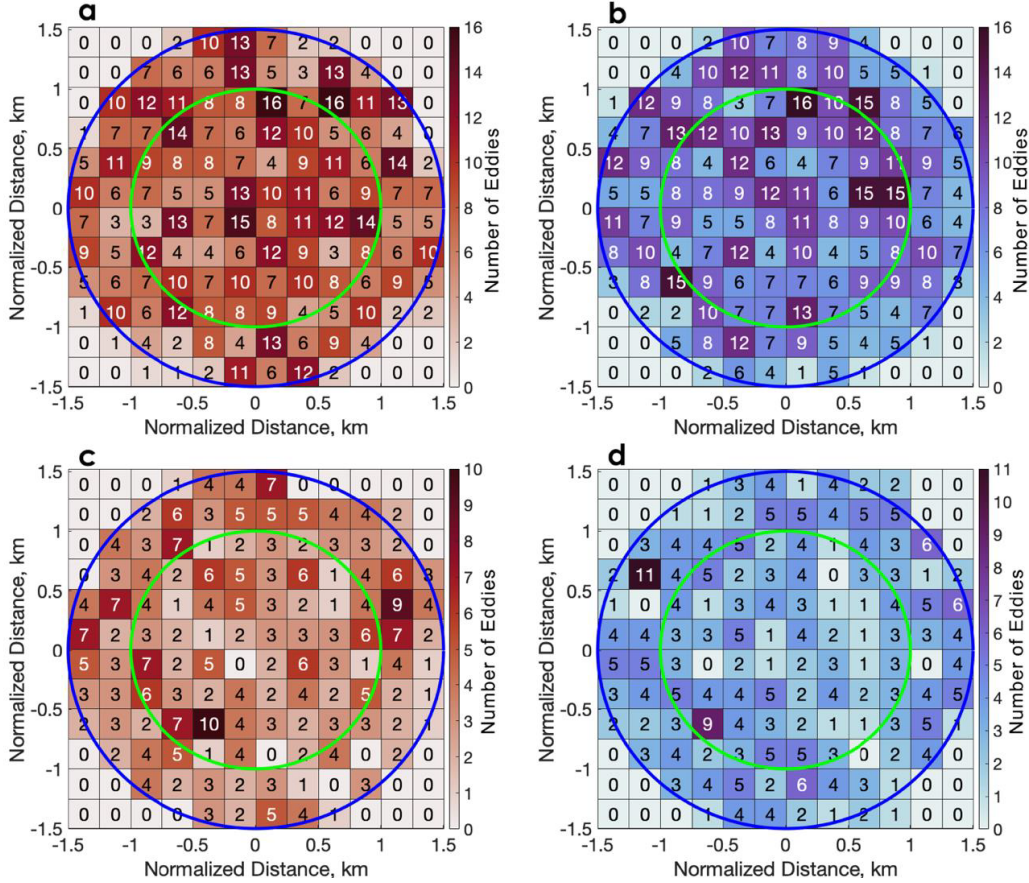
Figure 2. The distribution of the obtained profiles in the normalized eddy-coordinate system calculated in the $0.25R \times 0.25R$ bin associated with AEs (a, c) and CEs (b, d) eddies, in the Region I (a, b) and II (c, d). The green and blue circles indicate distance of $1R$ and $1.5R$ from the eddy center respectively.

trajectories instead of propagation velocity [e.g. *Dong et al.,* 2014]. Taking into account the spatial resolution of SLA gridded data and difference in size between latitude and longitude for the study region, the study area was divided into $1° \times 0.8°$ grid cells. For every cell, the number of eddies crossing the cell boundaries were tracked (i.e., western/eastern boundary for zonal transport and northern/southern boundary for meridional transport).

Transport (D) is calculated as $D = (VN)/M$, where D is the volume of water transported by a single composite eddy, N is the number of detected eddies that crossed the cell boundary and M is the time of the analysis period. Westward and northward transports are defined as positive. For every cell the zonal (resp., meridional) volume transport was calculated as an average between transports of the western and eastern (resp., northern and southern) borders of the cell.

Since the properties of rings formed in the Agulhas Retroflection region may significantly differ from the mesoscale eddies which form in other parts of the Agulhas Current System the study region was divided into the two subregions (Figure 1). Region I defined as 13°–22°E, 34°–41°S. It includes the Agulhas Leakage region and southeastern part of the Cape Basin, which has been referred in the previous studies as the Cape Cauldron [*Boebel et al.,* 2003]. Generation sites and most of the propagation trajectories of the Agulhas Rings are bordered by the Region I [*Dencausse et al.,* 2010; *Malysheva et al.,* 2018]. Region II includes eddies formed in the area of Agulhas Return Current as well as eddies formed in the northeastern part of the shelf zone (22°–28°E, 34°–41°S). This region is influenced by the juxtaposition of the Agulhas Return Current with the Subtropical Convergence Zone [*Boebel et al.,* 2003]. For every selected region, trajectories of eddies formed in this

region were taken into account. Thus, we exclude any possible influence on the final result of eddies formed outside the boundaries of the selected region.

3. Mean Eddy Properties

Since the data set we use contains the latest information about the eddy properties we think it is necessary to refresh basic eddy statistics for the study region.

A total number of 2651 of eddies (1350 CEs and 1301 AEs) were detected in the study region for the period 1993–2018. The mesoscale eddies of both polarities are ubiquitous in the Agulhas region (Figure 3). The coastal zone is an exception but zero values here can be explained by the gaps in the SLA fields near the coast due to the errors in SLA data in these areas. The maximum density of AEs is observed in the northeastern part of the shelf (Figure 3c, Figure 3d). The density of both AEs and CEs is minimal in the southern part of the shelf zone.

The patterns of eddy generation (locations where eddies were first detected by automatic identification algorithm) are presented in Figure 3a, Figure 3b. In general, eddies are formed almost everywhere in the study region. However, eddies are most frequently observed in the area to the west of the Agulhas Plateau (22°–24°E), in the Agulhas Retroflection region, and in the eastern part of the shelf zone. The latter pattern of the eddy genesis can be linked to the strong baroclinic instability of the Agulhas Current near the shelf area [*Wells et al.,* 2000]. The geographic distribution of eddy genesis for the AEs and CEs is generally similar, but CEs are formed closer to the western extremity of the Agulhas Plateau (Figure 3b).

The spatial patterns of eddy dissipation are presented in Figure 3e, Figure 3f). The main "eddy graveyards" are located to the west and to the east of the longitude band 20°–23°E. The eastern area of the shelf zone is also characterized by the high intensity of the dissipation processes. The patterns of eddy dissipation for both AEs and CEs can be linked to the topographic barriers, such as the Agulhas Plateau or the Agulhas Ridge, which cross the typical trajectories of the eddy propagation in the study area. This confirms the conclusions of previous studies about the significant influence of bottom topography on the eddy propagation and dissipation in the Agulhas region [*Hall and Lutjeharms,* 2011; *Schouten et al.,* 2000].

The average lifespan of the eddies formed in the study region is 132 days but it varies in the wide range and can reach 800 days. We normalize the eddy parameters by their lifetime where normalized lifetime 0 corresponds to the beginning of the eddy lifecycle, while normalized lifetime 1 corresponds to the end of the eddy lifespan. Thus, we obtain the distribution of the eddy parameters as a function of lifetime which allows us to analyze the time evolution of the mean eddy parameters for the study region (Figure 4).

Radius, amplitude and circum-averaged speed of the eddies of both polarities (Figure 4a, Figure 4b, Figure 4d) show dome-shape patterns of their temporal evolution with the minimum at the beginning of the eddy lifecycle. On the contrary, the propagation speed ($\sim$ 9 cm/s) is the strongest at the beginning of the eddy lifespan and rapidly decreases in the first 20% of the eddy lifecycle. The radius and circum-averaged speed of the AEs is larger than that of CEs throughout the eddy lifecycle while the amplitude of the CEs is mostly larger than for the AEs except at the first and last 5% of the eddy lifetime.

4. Radial Cross-Sections of the Composite Eddies

To analyze the vertical thermohaline structure of AEs and CEs in the study region the radial composite sections of temperature, salinity, and density anomalies were constructed based on the obtained three-dimensional composite structures. The radial cross-sections were calculated separately for Region I and II. Significant eddy-induced T'/S' anomalies are concentrated within the distance of one radius R from the eddy center. It should be also noted that composite eddies of both polarities significantly influence the thermohaline characteristics at the horizontal distance up to at least $1.5R$ from the eddy center (Figure 5, Figure 6).

4.1. Radial Cross-Sections in the Region I

The positive temperature anomalies in the composite AE are concentrated within the depth range of 100–700 m. The eddy core is located at a depth
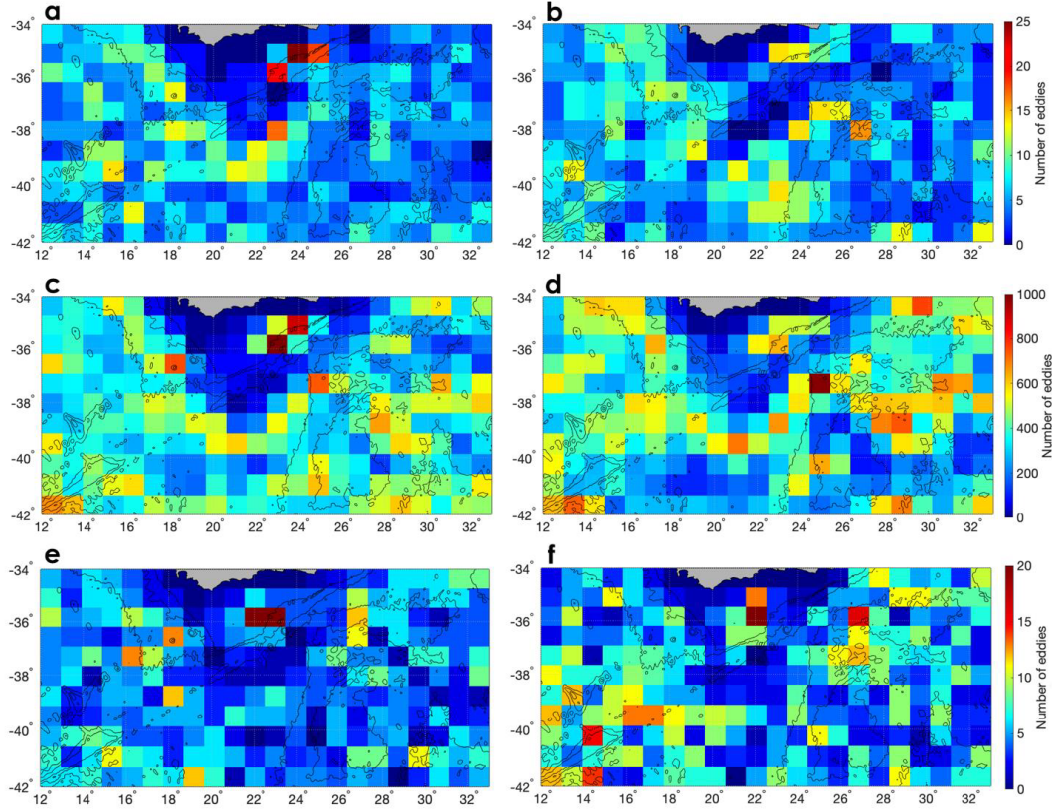
Figure 3. Geographic distributions of eddy genesis (a, b) occurrence (c, d) and dissipation (e, f) for the AEs (a, c, e) and CEs (b, d, f) (number of eddies for every $1° \times 0.8°$ bin for the period 1993–2018).

of 200 m with a maximum of about 1.94°C (Figure 5a). The penetration depth of the positive temperature anomalies in the composite AE reaches 1500 m. Nevertheless, even at the maximum depth of 1500 m, the temperature anomaly is no less than 0.2°C. The distribution of the salinity anomalies in the composite AE shows a similar pattern. However, the maximum penetration depth of salinity anomalies reaches 900 m (Figure 5b) which is significantly smaller than for the temperature anomalies. The maximum salinity anomaly is located at a depth of 400 m and equals 0.23 g/kg. The radial density structure of the composite AE mostly follows the temperature anomaly pattern with the maximum located at the depth of ~ 200 m. The negative density anomaly reaches the depth of 1500 m (Figure 5c).

The layer 150–700 m (Figure 5d) bound the core of the composite CE. The minimum value of temperature (salinity) anomaly is at a depth of 450 m (350 m) and equals −2.5°C (−0.25 g/kg) (Figure 5e). The penetration depth of significant salinity and temperature anomaly in the composite CE is 1500 and 800 m respectively.

4.2. Radial Cross-Sections in the Region II

Figure 6 shows the radial cross-sections of the composite eddies for Region II (Figure 1). The temperature core in the composite AE is located in the depth range of 200–800 m (Figure 6a) with a maximum value of 1.17°C located at the 600 m. The maximum salinity anomaly is 0.15 g/kg at a depth of 400 m (Figure 6b). The vertical penetration depth of significant temperature/salinity anomalies for the composite AE and CE is 1400/800 m and 1250/700 m respectively.

The depth of the eddy core in the composite CE is about 400 m (Figure 6d) with the minimum temperature and salinity anomaly of −1.38°C and −0.17 g/kg located at the 400 m and 250 m respectively. The eddy core also manifests itself in the density field (Figure 6f).

Although the general thermohaline structure of the radial cross-sections for the composite AE and CE shows a similar to Region I pattern, the average
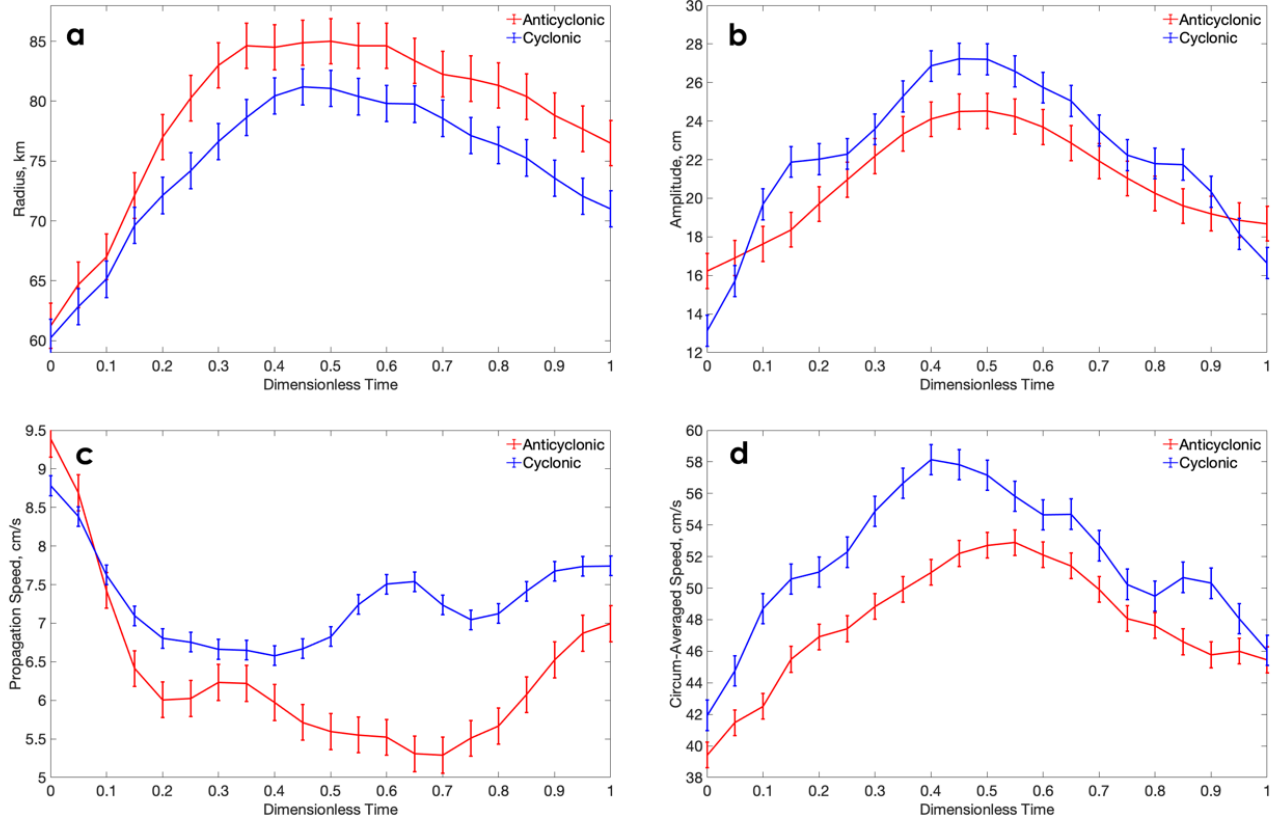
Figure 4. Mean eddy radius (a), amplitude (b), propagation speed (c) and circum-averaged speed as a function of the normalized eddy lifetime. The error bars denote the standard error of the mean.

T'/S' values for the two regions differ significantly. Maximum T'/S values for the composite AE in Region I are ~ 1.5 times higher than maximum T'/S values for the composite AE in Region II. Similar ratios are observed for the average T'/S values of the composite CE from the two regions.

5. Three-Dimensional Structures of the Composite Eddies

Figure 7, Figure 8 show three-dimensional structures of a composite AE and CE for Region I and horizontal distributions of temperature and salinity anomalies at selected depth levels. The shape of the AE core is close to symmetrical and maximum values of the temperature and salinity anomalies are concentrated in the geometrical center of the eddy (Figure 7). The core of the composite AE has a distinctive structure which is prominent feature of the Agulhas Rings [*Laxenaire et al.*, 2019]. Starting from a depth of about 500 m the eddy signature in the temperature and salinity fields is gradually decreasing. This reduction manifests itself both in the decreasing of temperature/salinity anomalies with depth and in the decreasing of the distribution of significant ($> 0.1°C$) anomalies from the eddy center. At the depth of 1000 m, significant temperature anomalies extend at the distance of $0.5R$.

There is a small asymmetry in the three-dimensional structure of the AE. Temperature extrema are shifted at $\sim 0.25R$ to the north from the eddy center (Figure 8). This asymmetry is gradually decreasing with depth and insignificant at the 800 m. It should be also noted that in both composite AE and CE in the surface layer (down to 50 m) the temperature and salinity anomalies almost undetectable and sharp increase of the thermohaline anomalies starts from the depth level of about 100 m. This pattern can be tracked in both
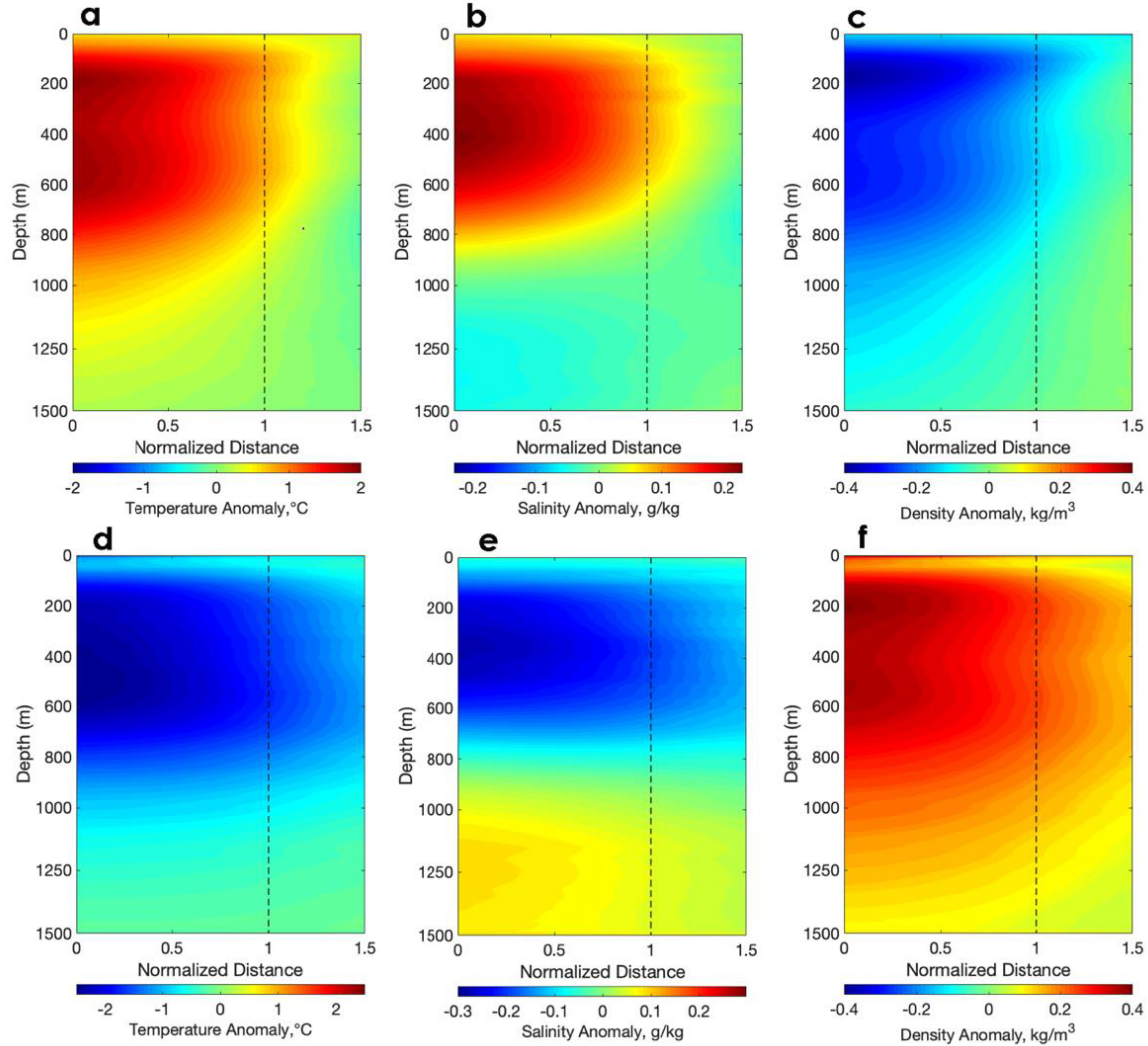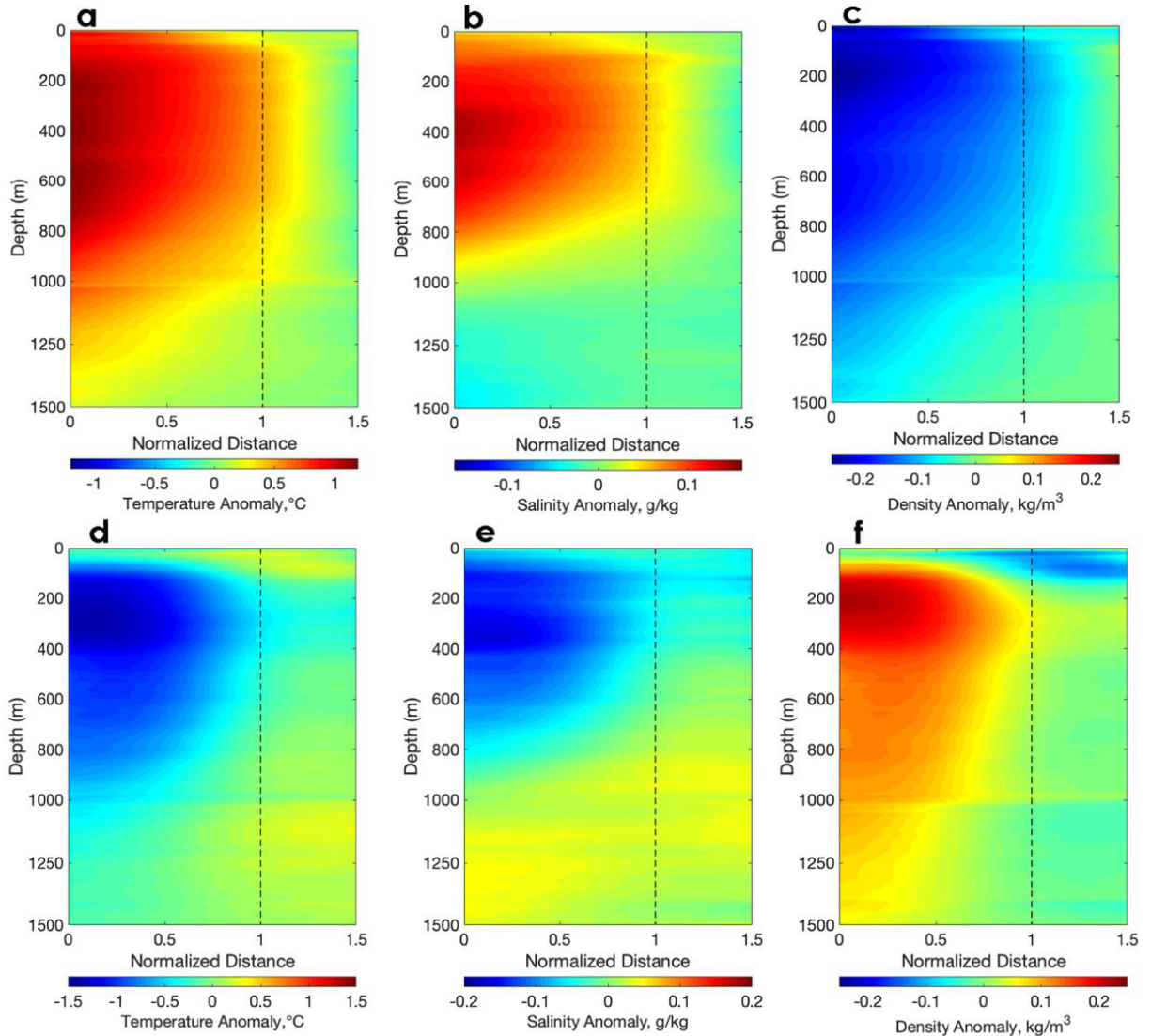
Figure 5. Radial cross-sections of temperature (a, d), salinity (b, e) and density (c, f) anomalies in the composite AE (top) and CE (bottom) (Region I).

radial cross-sections and three-dimensional structures (Figure 7, Figure 8). *Laxenaire et al.* [2019] showed that for the eddies in the Agulhas region in the layer of $\sim$ 0–150 m the strong seasonal signal is observed and specifically for the Agulhas Rings the water in this layer is not a part of the eddy core.

The composite AE in the Region II has an asymmetric spatial distribution of T'/S' values with extremum (maximum of T'/S') shifted at $\sim$ 0.5R to the northwest direction relative to the eddy center (Figure 9). The observed shift gradually decreasing with depth and equals about 0.25R at the 500 m. The opposite extremum (minimum of T'/S') of about $-2°$C$/-0.2$ g/kg is observed in the southeastern part of the composite eddy (Figure 9). The spatial distribution of the thermohaline anomalies

in the composite CE in the Region II (Figure 10) shows the similar symmetrical pattern with the composite CE in the Region I.

Figure 11 shows the vertical profiles of the temperature, salinity and density anomalies obtained by the horizontal averaging of all profiles located within the distance of 1R from the centers of AEs and CEs for the Regions I and II. We can see characteristic features of thermohaline eddy structure previously observed in the radial sections. The largest mean temperature anomalies in the composite AE are located within depth range of 200–600 m ($\sim$ 1.25°C) and 200–700 m ($\sim$ 0.65°C) in the Region I and II respectively. The minimum temperature anomalies in the composite CE are found at the $\sim$ 600 m for the Region I ($-1.9°$C)

Figure 6. Radial cross-sections of temperature (a, d), salinity (b, e) and density (c, f) anomalies in the composite AE (top) and CE (bottom) (Region II).

and at ~ 300 m for the Region II ($-1.45°$C). The extrema of T'/S' values in the composite AE are located at the depth level of about 400 m (0.15 g/kg and 0.08 g/kg for the Region I and II respectively). The extrema in the composite CE are found at the depth of 400 m (-0.2 g/kg) and 350 m (-0.18 g/kg) for the Regions I and II respectively (Figure 11b, Figure 11e). The profiles of mean density anomalies are mostly consistent with temperature anomalies which again demonstrates that density distribution of the study area is mostly driven by the temperature anomalies (Figure 11c, Figure 11f).

We can see that extrema of temperature, salinity and density anomalies in the CEs exceed in the absolute values the corresponding extrema in the AEs. This creates an asymmetry in the distribution of the thermohaline anomalies with a large shift towards negative temperature and salinity anomalies and positive density anomalies. This asymmetry is particularly prominent in eddy structures for Region I. It should also be noted that the averaged values of temperature and salinity anomalies in composite CE change the sign at a depth of about 1000 m. This feature is observed in composite CEs for both regions (Figure 11b, Figure 11e).
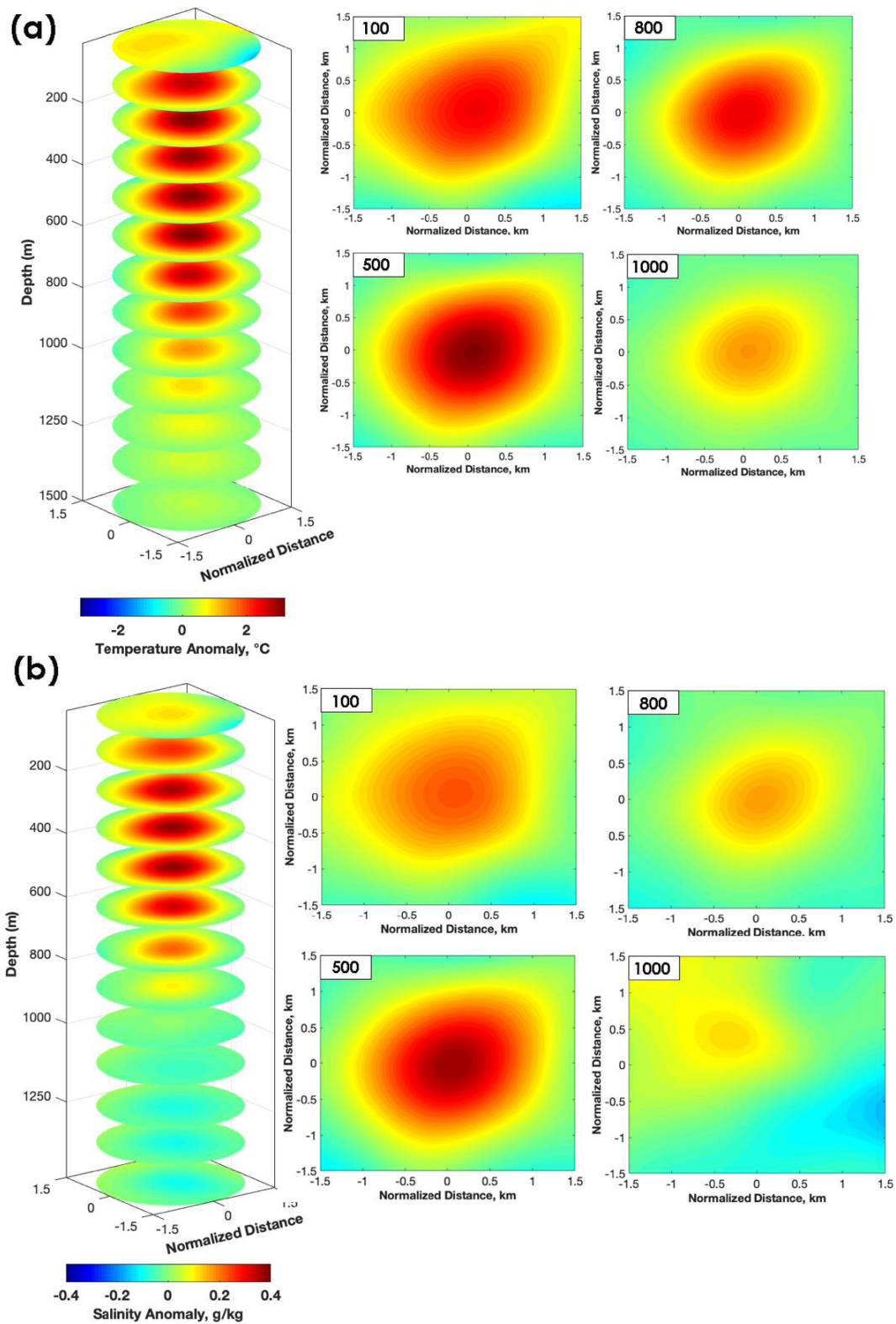
Figure 7. Three-dimensional temperature (a) and salinity (b) structure of the composite AE and horizontal distribution of temperature and salinity anomalies at the 100, 500, 800 and 1000 m (Region I). The x and y coordinates are normalized by eddy radius as in Figure 2.
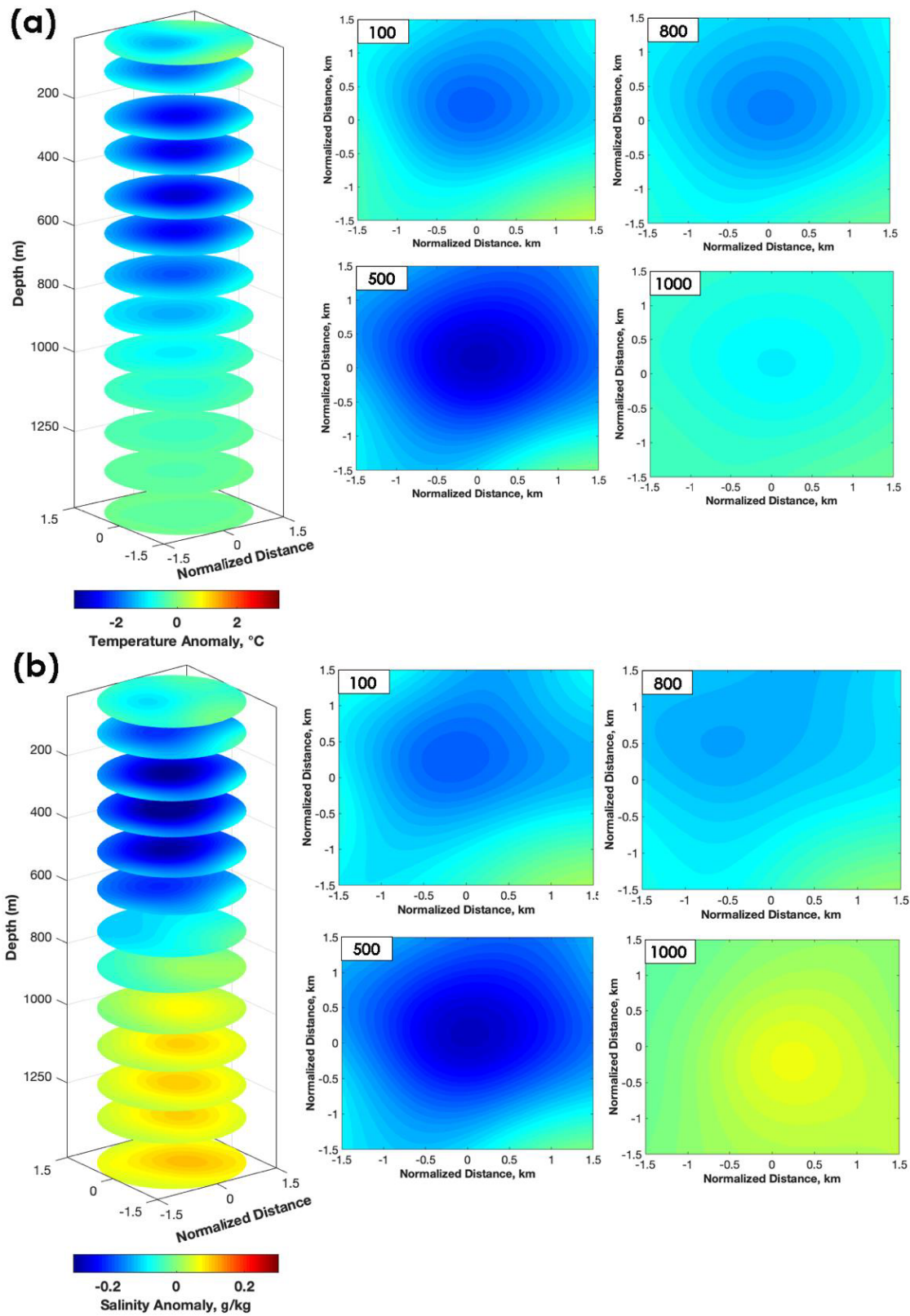
Figure 8. Three-dimensional temperature (a) and salinity (b) structure of the composite CE and horizontal distribution of temperature and salinity anomalies at the 100, 500, 800 and 1000 m (Region I). The x and y coordinates are normalized by eddy radius as in Figure 2.
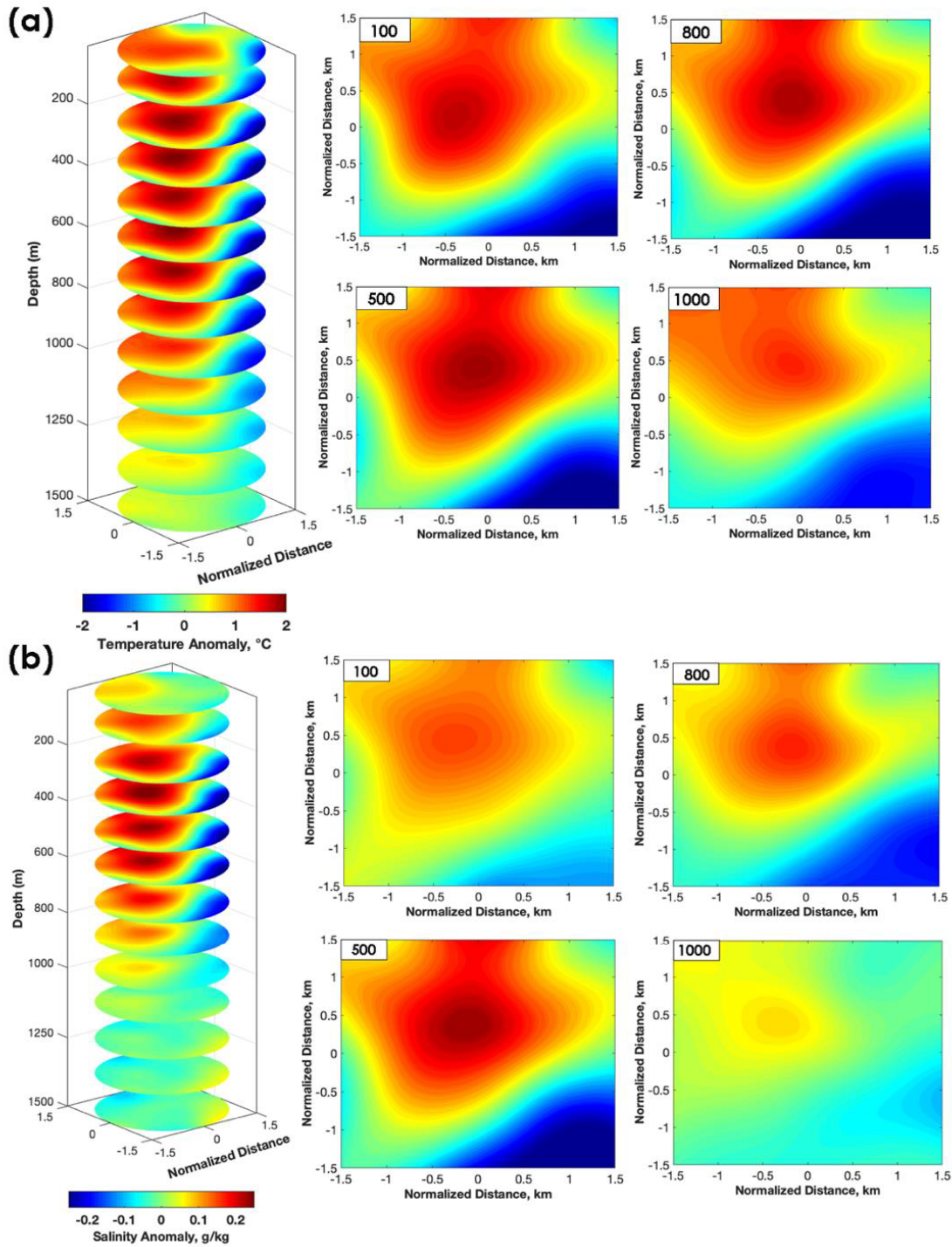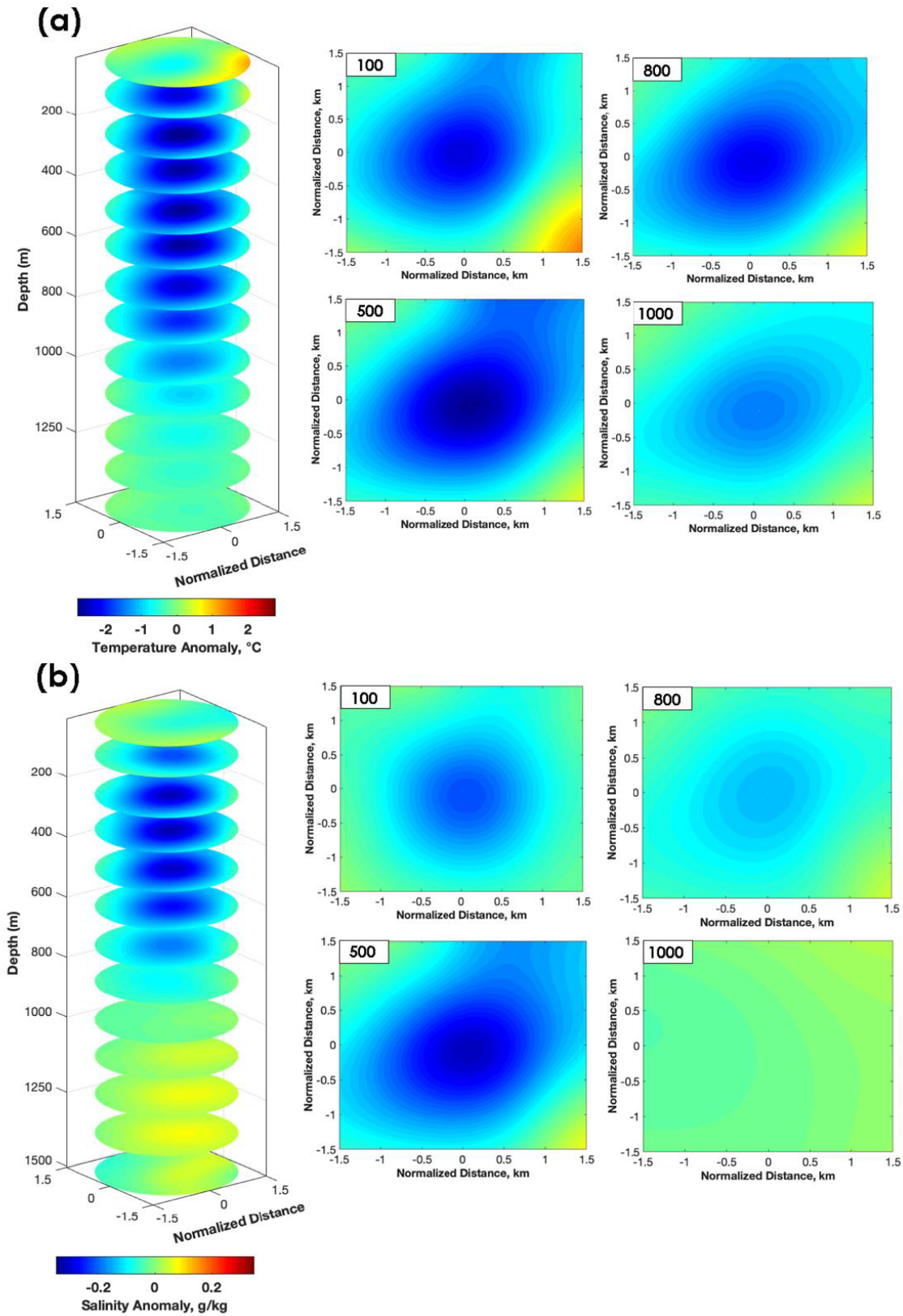
Figure 9. Three-dimensional temperature (a) and salinity (b) structure of the composite AE and horizontal distribution of temperature and salinity anomalies at the 100, 500, 800 and 1000 m (Region II). The x and y coordinates are normalized by eddy radius as in Figure 2.

Figure 10. Three-dimensional temperature (a) and salinity (b) structure of the composite CE and horizontal distribution of temperature and salinity anomalies at the 100, 500, 800 and 1000 m (Region II). The x and y coordinates are normalized by eddy radius as in Figure 2.
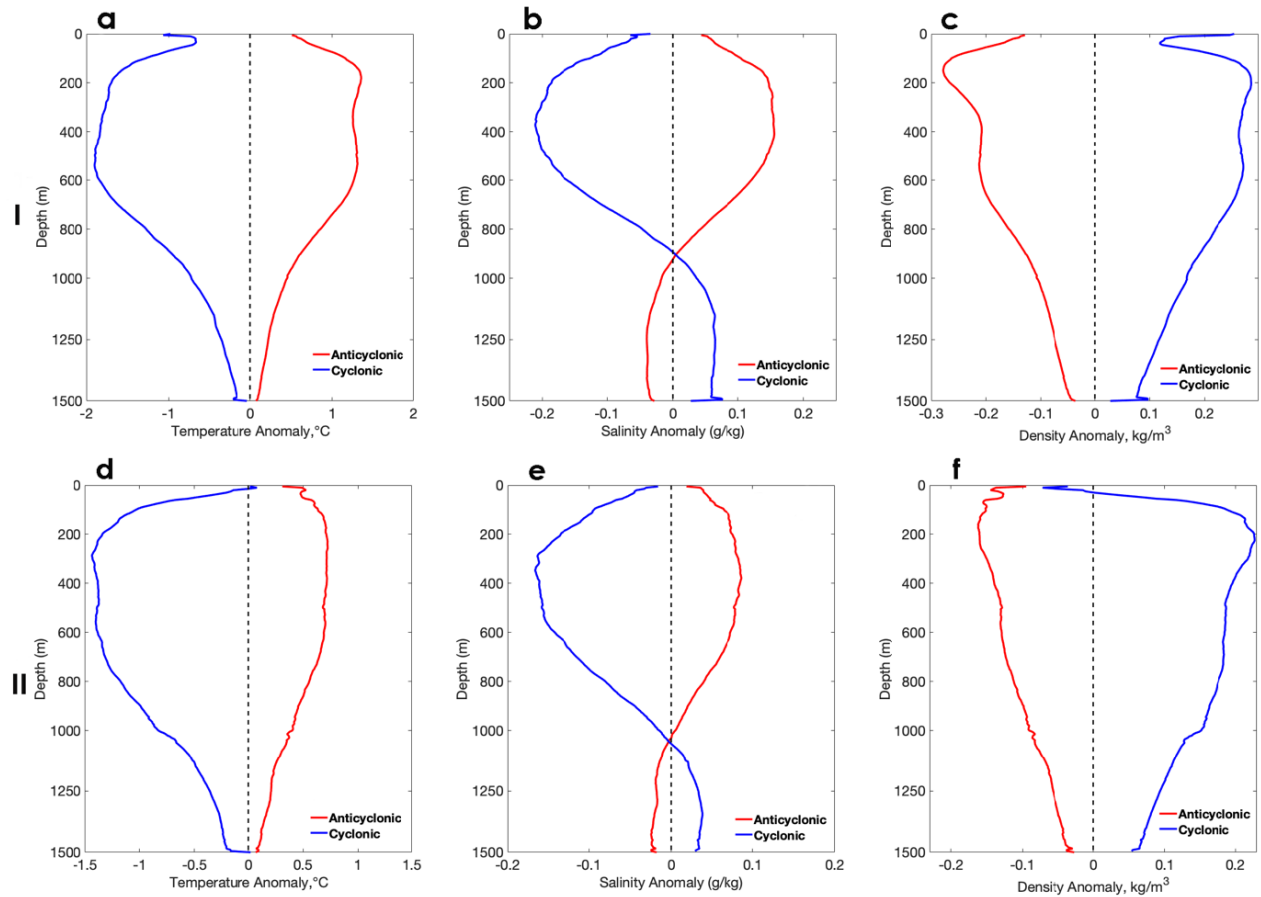
Figure 11. Mean vertical profiles of temperature (a), salinity (b) and density (c) anomalies averaged within $1R$ for the composite AE and CE (Region I and II).

## 6. Volume Transport and Heat and Salt Contents

Based on the obtained three-dimensional structures we estimate volume, heat, and salt transported by the mesoscale eddies in the study region Table 1. The average radius of the AEs (according to the Mesoscale Eddy Trajectory Atlas) is 96.2 ± 26.9 km in the Region I and 87.5 ± 27.3 km in the Region II. The average radius of the CEs is 84.8 ± 26.7 km and 73.4 ± 23.4 km in Region I and II respectively.

Defining the lower boundary of the eddy is a challenging task. By the "lower boundary" of the eddy we mean the depth down to which eddy trap volume, heat, salt, and biogeochemical constituents. Different studies follow different approaches but in general, they all come down to the two methods. The first method is defining the specific isotherm (or isohaline) as the threshold value defining the lower boundary of the eddy [*Belonenko et al.*, 2020; *Kubryakov et al.*, 2018; *Travkin and Belonenko*, 2019]. This approach can be implemented along with a detailed analysis of the water masses transported by the eddies in the specific region. To define the lower eddy boundary using the second approach we need to estimate the ratio of the orbital eddy velocity (v) and propagation speed of the eddy (c). In this case, the trapping depth is defined as a depth where the ratio v/c equals zero [*Chaigneau et al.*, 2011; *Flierl*, 1981]. The estimation of trapping depth of the Agulhas Rings plays a crucial role in the assessment of the Agulhas Leakage and ranges from 670 m to 1600 m in various studies [*Duncombe Rae et al.*, 1992; *McCartney and Woodgate-Jones*, 1991; *Schmid et al.*, 2003; *Van Sebille et al.*, 2010; *Laxenaire et al.*, 2019]. The broad range in the estimations of the trapping depth of the rings is due to the variation

Table 1. Characteristics of a Composite AE and CE in the Region I and II

| | Region I | | Region II | |
	AE	CE	AE	CE
Volume (10^{13} m^3)	3.49	2.71	2.4	1.69
HC (10^{20} J)	2.38	-1.9	1.12	-1.26
SC (10^{12} kg)	4.79	-3.07	2.69	-2.73
Volume transport (Sv)	5.89	4.88	4.11	3.89
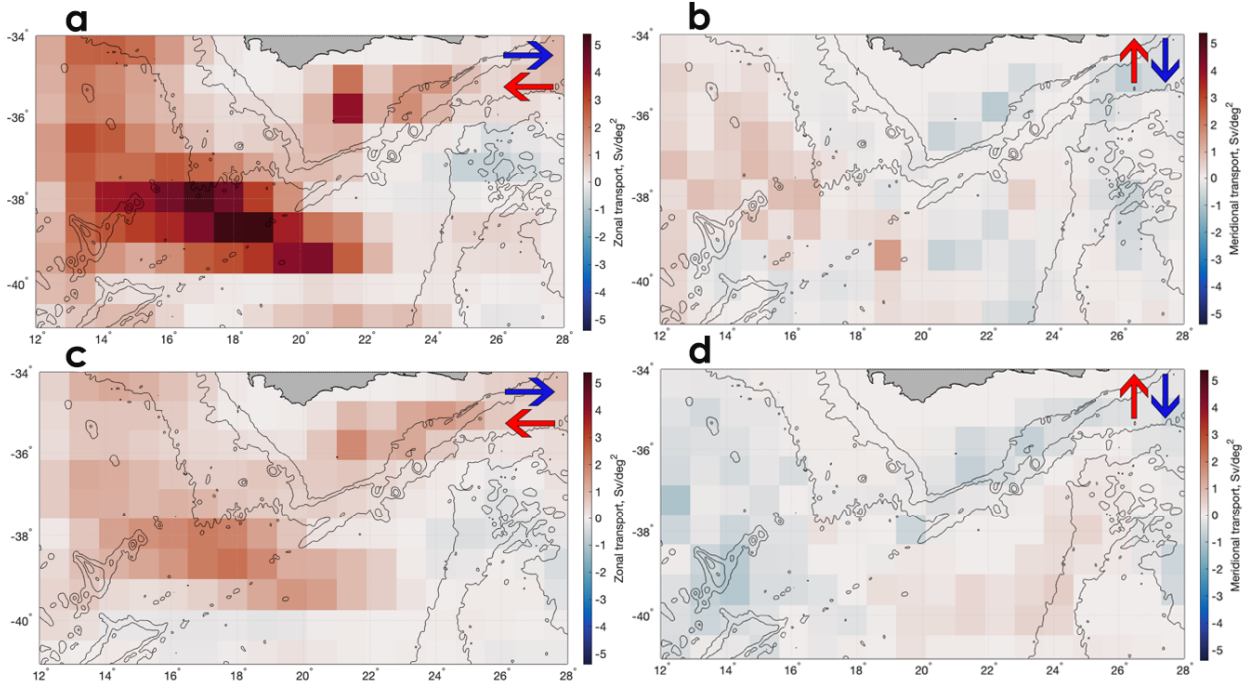
Figure 12. Zonal (a, c) and Meridional (b, d) eddy volume transport for the AEs (a, b) and CEs (c, d) calculated for every $1° \times 0.8°$ bin in the Agulhas Current region. The positive value refers to the westward transport; the negative value refers to the eastward transport.

of the spatial scales for the individual rings, as well as their dynamic and thermohaline characteristics. In this study, the lower boundary of the obtained composite eddy is defined as the location of the T'/S' value the corresponding to about 10% of the maximum T'/S' associated with eddies.

The lower boundary of the composite AE in the Region I is about 1200 m. For the composite AE and CE in the Region II the location of the trapping depth is ~ 1000 m. Thus, the mean eddy volume in Region I is 3.49×10^{13} m^3 for the composite AE and 2.71×10^{13} m^3 for the composite CE. For Region II this estimation is 2.4×10^{13} m^3 and 1.69×10^{13} m^3 for the composite AE and CE respectively. According to the Mesoscale Eddy Tra-

jectory Atlas Product, the average eddy propagation speed is 0.05/0.048 m/s and 0.047/0.053 m/s for Region I and II respectively.

The total heat (HC) and salt (SC) contents transported by the composite AE and CE were calculated as follows [*Chaigneau et al.,* 2011; *Dong et al.,* 2017]:

$$HC = \rho C_p \int T' dx dy dz$$

$$SC = \rho C_p \int S' dx dy dz$$

where $Cp = 4200$ J/kg K and $\rho = 1025$ kg/m^3 are specific heat capacity of the seawater and mean

upper ocean density respectively; T' is the eddy-induced temperature anomaly, S' is the eddy-induced salinity anomaly.

In various studies, the estimates of the volume of the Agulhas Rings range from 1.53×10^{13} m^3 to 7.1×10^{13} m^3 [*van Ballegooyen et al., 1994*; *Garzoli et al., 1999*; *Laxenaire et al., 2019 McDonagh et al., 1999*; *McCartney and Woodgate-Jones, 1991*; *Malysheva et al., 2018*; *Schmid et al., 2003*]. The obtained assessment of the volume of the Agulhas Ring (3.49×10^{13} m^3) is most consistent with the results of a study *McCartney and Woodgate-Jones* [1991] (3.6×10^{13} m^3). According to the number of studies the range of the estimates of the heat and salt transported by the Agulhas Rings is 0.19×10^{20} J $-$ 2.5×10^{20} J for the heat estimates and 1.21×10^{12} kg $-$ 13.1×10^{12} kg for the salt estimates [*van Ballegooyen et al., 1994*; *Duncombe Rae et al., 1996*; *Garzoli et al., 1999*; *Laxenaire et al., 2019*; *McCartney and Woodgate-Jones, 1991*; *McDonagh et al., 1999*; *Schmid et al., 2003*].

Our assessment of the heat and salt trapped by the composite AE in the Region I (2.38×10^{20} J and 4.79×10^{12} kg) is mostly consistent with the *van Ballegooyen et al.* [1994] (2.36×10^{20} J and 4.59×10^{12} kg).

Figure 12 shows spatial distributions of the mean zonal and meridional eddy induced transport for CEs and AEs for the study region. Zonal eddy-induced transport has a general westward direction for the eddies of both polarities. The maximum value of the zonal eddy-induced transport is 5.38 Sv/deg^2 in the Agulhas Retroflection region (Figure 12a).

Following the patterns of the zonal eddy-induced transport, we can track typical propagation trajectories of the Agulhas Rings from the Agulhas Retroflection region to the Cape Basin (Figure 12a). Westward propagation of the zonal transport for AEs and CEs is also observed in the central part of the shelf zone (Figure 12a, Figure 12c) with the maximum values of 4 Sv/deg^2 for AEs and 1.77 Sv/deg^2 for CEs. The eastern direction of the eddy-induced transport is predominant in the area of the Agulhas Return Current (across the $40°$S) and in the Agulhas Plateau region. At the northwest area of the Agulhas Plateau, the intensity of the eastern eddy-induced transport reaches 0.67 Sv/deg^2 for AEs and 0.68 Sv/deg^2 for CEs.

An interesting feature of the meridional eddy-induced transport in the study region is the predominance of the northward transport for AEs in the area of the Cape Basin and to the east of the Agulhas Plateau (Figure 12b), while for CEs the southward direction of the meridional transport prevails in this area (Figure 12d). The predominant southward direction of the meridional transport is also observed in the shelf zone.

7. Conclusion

By implementing the method of colocalization of the altimetry data and temperature and salinity profiles we obtained the averaged composite thermohaline structures of the AEs and CEs in the Agulhas Current region, as well as the averaged estimations of the heat and salt transported by the Agulhas Rings.

The use of satellite altimetry data along with the Argo profiles presents a powerful tool for obtaining the three-dimensional structures of the mesoscale eddies. It also provides the opportunity to assess an estimation of the inter-ocean exchange based on the eddy's volume and associated anomalies.

The observed intensification of eddy dissipation processes can be caused by the topographic barriers, such as the Agulhas Plateau or the Agulhas Ridge. *Schouten et al.* [2000] and *Hall and Lutjeharms* [2011] demonstrated that ridges connecting the African continent with the Mid-Atlantic Ridge in the South Atlantic significantly affect the propagation patterns of the mesoscale eddies in the Agulhas region. While crossing the ridges rings lose almost 70% of their kinetic energy and can split into smaller eddies most of which never leave the area of the Cape Basin [*Schouten et al., 2000*].

The internal structure of the obtained composite AE in Region I is characterized by a subsurface core which has been previously identified as Mode Waters [*Arhan et al., 1999*; *Laxenaire et al., 2019*; *Souza et al., 2018*]. This thick core accumulates the strongest heat and salt anomalies which are responsible for the advection of a large amount of heat and salt from the Indian Ocean to the South Atlantic Ocean. In both composite AE and CE in the surface layer (down to 50 m) the temperature and salinity anomalies almost undetectable and the rapid increase of the thermohaline anomalies starts from about 100 m. *Nencioli et al.* [2018] and *Laxenaire et al.* [2019] showed that for the eddies in

the Agulhas region in the layer of $\sim$ 0–150 m the strong seasonal signal is observed and specifically for the Agulhas Rings the water in this layer is not a part of the eddy core.

The temperature and salinity anomalies in the composite AE are concentrated within the depth range of 100–700 m and reach 1.94°C and 0.23 g/kg in Region I. For Region II the eddy core in the composite AE is located in the depth range of 200–800 m with a maximum value of 1.17°C and 0.15 g/kg. The core of the composite CE in the Region I concentrated in the layer 150–700 m with the temperature and salinity anomalies reach -2.5°C and -0.25 g/kg respectively. The depth of the eddy core in the Region I in the composite CE is about 400 m with the minimum temperature and salinity anomaly of -1.38°C and -0.17 g/kg located at 400 m and 250 m respectively.

The estimation of the average volume of the Agulhas Rings (composite AE in Region I) based on the obtained composite structure is consistent with the results of a study *McCartney and Woodgate-Jones* [1991]. Our assessment of the heat and salt trapped by the composite AE in Region I $(2.38 \times 10^{20}$ J and 4.79×10^{12} kg) is mostly consistent with the *van Ballegooyen et al.* [1994] $(2.36 \times 10^{20}$ J and 4.59×10^{12} kg).

Westward propagation of the zonal eddy-induced transport for AEs and CEs is observed in the Agulhas Retroflection region, Cape Basin, and in the central part of the shelf zone with the maximum values of 4 Sv/deg^2 for AEs and 1.77 Sv/deg^2 for CEs. The eastern direction of the eddy-induced transport is predominant in the area of the Agulhas Return Current and in the Agulhas Plateau region. A prominent feature of the meridional eddy-induced transport in the study region is the predominance of the northward transport for AEs in the area of the Cape Basin and to the east of the Agulhas Plateau while for CEs the southward direction of the meridional transport prevails in this area.

From the patterns of the zonal eddy induced transport (Figure 12) we can see the typical paths of the eddy propagations from the Agulhas Retroflection region to the Cape Basin which are associated with the Agulhas Leakage. This process plays a significant role in climate variability and predictability and impacts the Atlantic meridional overturning circulation (AMOC).

References

Arhan, M., H. Mercier, J. R. E. Lutjeharms (1999), The disparate evolution of three Agulhas rings in the South Atlantic Ocean, *Journal of Geophysical Research Oceans*, *104*, No. C9, 987, **Crossref**

van Ballegooyen, R. C., et al. (1994), Eddy fluxes of heat and salt from the southwest Indian Ocean into the southeast Atlantic Ocean: A case study, *Journal of Geophysical Research*, *99*, No. C7, 14,053–14,070, **Crossref**

Barnes, S. L. (1973), *Mesoscale objective map analysis using weighted time-series observations (NOAA Tech. Memo. ERL NSSL-69*, 60 pp. National Severe Storm Laboratory, Norman, OK.

Belonenko, T., V. Zinchenko, et al. (2020), Evaluation of Heat and Salt Transports by Mesoscale Eddies in the Lofoten Basin, *Russ. J. Earth Sci.*, *20*, ES6011, **Crossref**

Boebel, O., J. R. E. Lutjeharms, et al. (2003), The Cape Cauldron: a regime of turbulent inter-ocean exchange, *Deep-Sea Research II*, *50*, No. 1, 57–86, **Crossref**

Byrne, D. A., A. L. Gordon, W. F. Haxby (1995), Agulhas eddies: A synoptic view using Geosat ERM data, *Journal of Physical Oceanography*, *25*, No. 5, 902917, **Crossref**

Chaigneau, A., M. Le Texier, et al. (2011), Vertical structure of mesoscale eddies in the eastern South Pacific Ocean: A composite analysis from altimetry and Argo profiling floats, *J. Geophys. Res.*, *116*, C11025, **Crossref**

Chelton, D. B., M. G. Schlax, R. M. Samelson (2011), Global observations of nonlinear mesoscale eddies, *Prog. Oceanogr.*, *91*, 167–216, **Crossref**

Chelton, D. B., M. G. Schlax, et al. (2007), Global observations of large oceanic eddies, *Geophysical Research Letters*, *34*, 15, **Crossref**

Dencausse, G., M. Arhan, S. Speich (2010), Routes of Agulhas rings in the southeastern Cape Basin, *Deep Sea Research Part I: Oceanographic Research Papers*, *57*, No. 11, 1406–1421, **Crossref**

Dong, D., P. Brandt, et al. (2017), Mesoscale eddies in the Northwestern Pacific Ocean: Three-dimensional eddy structures and heat/salt transports, *Journal of Geophysical Research: Oceans*, *122*, 9795–9813, **Crossref**

Dong, C., J. C. McWilliams, et al. (2014), Global heat and salt transports by eddy movement, *Nature Communications*, 3294, **Crossref**

Duncombe Rae, C., F. Shillington, et al. (1992), An Agulhas ring in the South Atlantic Ocean and its interaction with the Benguela upwelling frontal system, *Deep Sea Research Part A. Oceanographic Research Papers*, *39,* 2009–2027, **Crossref**

Duncombe Rae, C., S. Garzoli, A. Gordon (1996), The eddy field of the southeast Atlantic Ocean: A statistical census from the Benguela Sources and Transports Project, *J. Geophys. Res.: Oceans*, *101,* No. C5, 11,949–11,964, **Crossref**

Flierl, G. R. (1981), Particle motions in large-amplitude wave fields, *Geophys. Astrophys. Fluid Dyn.*, *18,* 39–74, **Crossref**

Garzoli, S. L., P. L. Richardson, et al. (1999), Three Agulhas rings observed during the Benguela Current Experiment, *Journal of Geophysical Research*, *104,* 20,971–20,985, **Crossref**

Gordon, A. L., J. R. Lutjeharms, M. L. Griindlingh (1987), Stratification and circulation at the Agulhas Retroflection, *Deep Sea Research Part A. Oceanographic Research Papers*, *34,* No. 4, 565–599, **Crossref**

Hall, C., J. R. E. Lutjeharms (2011), Cyclonic eddies identified in the Cape Basin of the South Atlantic Ocean, *J. Marine Systems*, *85,* 1–10, **Crossref**

He, Q., H. Zhan, et al. (2018), A new assessment of mesoscale eddies in the South China Sea: Surface features, three-dimensional structures, and thermohaline transports, *Journal of Geophysical Research: Oceans*, *123,* 4906–4929, **Crossref**

Keppler, L., S. Cravatte, et al. (2018), Observed characteristics and vertical structure of mesoscale eddies in the southwest tropical Pacific, *Journal of Geophysical Research: Oceans*, *123,* 2731–2756, **Crossref**

Kubryakov, A. A., A. V. Bagaev, et al. (2018), Thermohaline structure transport and evolution of the Black Sea eddies from hydrological and satellite data, *Progress in Oceanography*, *167,* 44–63, **Crossref**

Laxenaire, R., S. Speich, S. Alexandre (2019), Evolution of the thermohaline structure of one Agulhas Ring reconstructed from satellite altimetry and Argo floats, *Journal of Geophysical Research: Oceans*, *124,* 8969–9003, **Crossref**

Lutjeharms, J. R. E. (2006), *The Agulhas Current*, 330 pp. Springer, Berlin, Heidelberg.

Lutjeharms, J. R. E. (2007), Three decades of research on the greater Agulhas Current, *Ocean Science*, *3,* No. 1, 129–147, **Crossref**

Lutjeharms, J. R. E., R. C. van Ballegooyen (1988), The retroflection of the Agulhas Current, *J. Physical Oceanography*, *18,* 1570–1583, **Crossref**

Lutjeharms, J. R. E., H. R. Valentine (1988), Evidence for persistent Agulhas rings southwest of Cape Town, South African, *J. Science*, *84,* 781–783.

Malysheva, A. A., A. V. Koldunov, et al. (2018), Agulhas Leakage Eddies based on the altimetry data, *Uchjonye Zapiski RGGMU*, *52,* 154–170. (in Russian)

McCartney, M. S., M. Woodgate-Jones (1991), A deep-reaching anticyclonic eddy in the subtropical gyre of the eastern South Atlantic, *Deep Sea Research Part A. Oceanographic Research Papers*, *38,* 411–443, **Crossref**

McDonagh, E. L., K. J. Heywood, M. P. Meredith (1999), On the structure, paths, and fluxes associated with Agulhas rings, *Journal of Geophysical Research: Oceans*, *104,* No. C9, 21,007–21,020, **Crossref**

Monin, A. S., G. M. Zhiharev (1990), Ocean Eddies, *Uspekhi Fizicheskikh Nauk*, *160,* No. 5, 1–47, (in Russian)**Crossref**

Nencioli, F., G. Dall'Olmo, G. D. Quartly (2018), Agulhas ring transport efficiency from combined satellite altimetry and Argo profiles, *Journal of Geophysical Research: Oceans*, *123,* No. 8, 5874–5888, **Crossref**

Sandalyuk, N. V., T. V. Belonenko (2018), Mesoscale vortex dynamics in the Agulhas Current from satellite altimetry data, *Sovremennye Problemy Distantsionnogo Zondirovaniya Zemli iz Kosmosa*, *15,* No. 5, 179–190, (in Russian)**Crossref**

Sandalyuk, N. V., A. Bosse, T. V. Belonenko (2020), The 3-D structure of mesoscale eddies in the Lofoten Basin of the Norwegian Sea: A composite analysis from altimetry and in situ data, *Journal of Geophysical Research: Oceans*, *125,* e2020JC016331, **Crossref**

Schmid, C., O. Boebel, W. Zenk, et al. (2003), Early evolution of an Agulhas Ring, *Deep Sea Research Part II: Topical Studies in Oceanography*, *50,* No. 1, 141–166, **Crossref**

Schouten, M. W., W. P. M. de Ruijter, et al. (2000), Translation, decay and splitting of Agulhas rings in the southeastern Atlantic Ocean, *Journal of Geophysical Research*, *105,* No. C9, 21,913–21,925, **Crossref**

van Sebille, E., P. J. van Leeuwen (2007), Fast northward energy transfer in the Atlantic due to Agulhas rings, *Journal of Physical Oceanography*, *37,* No. 9, 2305–2315, **Crossref**

van Sebille, E., P. J. van Leeuwen, et al. (2010), On the fast decay of Agulhas rings, *J. Geophys. Res.*, *115,* C03010, **Crossref**

Souza, J. M. A. C., C. de Boyer Montegut, et al. (2011), Estimation of the Agulhas ring impacts on meridional heat fluxes and transport using ARGO floats and satellite data, *Geophysical Research Letters*, *38,* L21602, **Crossref**

de Souza, A. G. Q., R. Kerr, J. L. L. de Azevedo (2018), On the influence of subtropical mode water on the South Atlantic Ocean, *Journal of Marine Systems*, *185,* 13–24, **Crossref**

Schlax, M. G., D. B. Chelton (2016), *The "Growing Method" of Eddy Identification and Tracking in Two and Three Dimensions*, College of Earth, Ocean and Atmospheric Sciences Oregon State University, Corvallis, Oregon.

Travkin, V. S.,   T. V. Belonenko (2019),   Seasonal variability of mesoscale eddies of the Lofoten Basin using satellite and model data, *Russian Journal of Earth Sciences*, *19,* No. 5,   ES5004,   **Crossref**

Wells, N. C.,   V. O. Ivchenko,   S. E. Best (2000), Instabilities in the Agulhas Retroflection Current system: A comparative model study, *J. Geophys. Res.*, *105,* No. C2,   3233–3241,   **Crossref**

Williams, S., M. Hecht, et al.   (2011), Visualization and analysis of eddies in a global ocean simulation, *Comput. Graphics Forum*, *30,*   991–1000,   **Crossref**

Willis, J. K.,   L.-L. Fu (2008),   Combining altimeter and subsurface float data to estimate the time-averaged circulation in the upper ocean, *J. Geophys. Res.*, *113,*   C12017,   **Crossref**

Yang, G., F. Wang, et al.   (2013),   Mesoscale eddies in the northwestern subtropical Pacific Ocean: Statistical characteristics and three-dimensional structures, *Journal of Geophysical Research: Oceans*, *118,* 1906–1925,   **Crossref**

Yu, L.-S.,   A. Bosse, et al.   (2017),   The Lofoten Basin eddy: Three years of evolution as observed by Seagliders, *J. Geophys. Res. Oceans*, *122,*   6814–6834,   **Crossref**

Zhang, Z.,   Y. Zhang, et al.   (2013),   Universal structure of mesoscale eddies in the ocean, *Geophys. Res. Lett.*, *40,*   3677–3681,   **Crossref**

Corresponding author:

Nikita Sandalyuk, Saint Petersburg State University, 7–9, Universitetskaya nab., Saint Petersburg 199034, Russia. (n.sandalyuk@spbu.ru)